Synthesis, characterization and reactivity study of nanoscale magnesium oxide

Fares Khairallah [1], Antonella Glisenti *

Dipartimento di Scienze Chimiche, Università degli Studi di Padova, Via Marzolo 1, 35131 Padova, Italy

Abstract

In this study, different samples of nanoscale magnesium oxide (MgO) were synthesized using "*aqueous wet chemical method (MgO-OX)*" and "*surfactant method (MgO-BR: surfactant used Brij 56, MgO-TR: surfactant used Triton 100-X)*". The samples were then characterized by: X-ray photoelectron spectroscopy (XPS), X-ray diffraction (XRD), diffuse reflectance infrared Fourier-transform (DRIFT) spectroscopy and Thermogravimetric analysis (TGA). From the analyses performed, it was noticed that the amount of hydroxyl and carbonate groups differs as a function of the synthesis procedure. The estimated dimensions of the particles are smaller in the MgO-OX sample (around 13 nm) compared to the 16 nm of the MgO-BR samples and 18 nm of the MgO-TR samples. Studies on the reactivity of MgO nanoparticles were performed using the DRIFT spectroscopy. Methanol and carbon monoxide were used to study the catalytic activity of MgO. At relatively low temperatures, methanol dissociates to methoxide species. At higher temperatures, different oxidation products (formates and formic acid, CO and CO_2) were observed to form. MgO-OX showed more oxidative properties than the MgO-TR/BR samples. Moreover, the basic and acidic sites were investigated using carbon dioxide and pyridine, respectively; the obtained results indicate a different distribution of acidic/basic sites in the different samples.
© 2007 Published by Elsevier B.V.

Keywords: Nanopowder; Magnesia; Magnesium oxide; Methanol oxidation; DRIFT; XPS

1. Introduction

Magnesium oxide is considered one of the most important compounds of magnesium industry. It is used in a variety of applications (refractory materials, pharmaceutical, waste remediation, glass industry and catalysis) [1,2]. MgO has a simple sodium-chloride structure and is very stable thermally and stoichiometrically. It has been reported that nanoscale MgO exhibits different reactivities from conventionally prepared MgO [3]. Previous works [3–5] have shown that nanocrystalline MgO exhibits remarkable reactivity and rates of adsorption primarily due to two main properties:

(a) huge surface areas;
(b) unusual crystal shapes with a high amount of coordinatively unsaturated edge/corner surface sites as well as defect sites that are more reactive toward incoming adsorbates.

This work presents a synthesis, characterization and reactivity study of nanoscale MgO samples synthesized using different methods. Reactivity studies were carried out through interactions with simple molecules (methanol and carbon monoxide). Moreover, an investigation on the basic and acidic sites present on the surface was performed by means of the chemisorption of probe molecules (carbon dioxide and pyridine). The interaction between MgO and several small molecules is an extensively investigated topic [6–33]; nevertheless, few papers are concerned with the influence of the preparation procedure on surface reactivity and, to our knowledge, this is particularly true for nanoscale MgO.

It is agreed that MgO prepared by different routes has different surface morphologies and properties and thus catalytic activity and selectivity may vary; other factors, such as the heating temperature, treatment times, pH, gelling agent, and the atmosphere in which the substance is heated affect greatly the activity of the final product [34,35].

Many different synthetic routes provide nanoscale MgO including sol–gel [2,36–41], hydrothermal [42], flame spray pyrolysis [43], laser vaporization [44], chemical gas phase deposition [45], combustion aerosol synthesis [46], aqueous wet

chemical [47] and surfactant methods [48]. . ., etc. The last two methods, adopted in this work, were selected on the basis of their simplicity and the relatively good control of the experimental procedure.

Methanol is a simple molecule commonly used as a probe. In addition, methanol is usually highly reactive toward metal oxides [49] and may be involved both in acid–base and redox equilibria generating different products (formaldehyde, formic acid, CO, CO_2, H_2O), depending on the nature of the active catalytic sites. Moreover, methanol is considered a promising combustible in fuel cell technology [49].

In basic research work carbon monoxide is frequently used as a model gas in adsorption and oxidation reactions on metal oxide surfaces [33,50]. CO is a very selective probe due to its weak interaction energy [51–53]; moreover, the C–O stretching frequency can give valuable information concerning the active sites. Earlier works [52,53] demonstrate that CO adsorption on MgO generates different species depending on the type of active sites present on the surface. Moreover, CO is important from the environmental point of view and for its use as a useful resource in chemical industries [54].

Carbon dioxide and pyridine (py) are considered probe molecules for the investigation of basic and acidic sites respectively. The CO_2 molecule has long been used as a probe for surface basicity of metal oxide powders [55–57]. The chemisorption of CO_2 on the surface of basic oxides leads to different compounds. This depends primarily on whether it interacts with hydroxyl groups (formation of hydrogen carbonate species) or with surface oxygen (formation of mono or bi-coordinated carbonates) [55,57–58]. The py adsorption is considered a complementation to CO_2 adsorption for the study of acid-base sites on the surface being adsorbed on both Brønsted- and Lewis-acid sites [59–61].

2. Experimental

2.1. "Aqueous wet chemical method" procedure [47]: MgO-OX

MgO was precipitated from a magnesium nitrate solution by means of ammonium hydroxide (pH 8–9). Tetraethylammonium hydroxide was added to facilitate gelation/precipitation. The obtained precipitate was dried and calcined in air at 550 °C for 4 h.

2.2. "Surfactant method" procedure [48]

The magnesium oxide samples prepared using "surfactant method" are denoted by MgO-BR (surfactant used: Brij 56, Aldrich) and MgO-TR (surfactant used: Triton X-100, Acros Organics).

A magnesium nitrate solution was added slowly to the surfactant liquid (80 °C) while stirring. The gel obtained at room temperature (RT) was then calcined for 4 h at 550 °C.

2.3. Characterization and reactivity

The DRIFT spectra were collected using a Bruker IFS 66 spectrometer by using a low temperature reaction chamber (CHC) installed in the Praying Mantis^{TM} accessory for diffuse reflection spectroscopy (HARRICK Scientific Co.). For the adsorption experiments, the sample was exposed to the reactive species at a flow rate of $100 \, cm^3 \, min^{-1}$ using the spectrum obtained before the exposure as a background spectrum. By means of this procedure only the species derived from the exposure are visible.

The CHC chamber was filled with the CO (Air Liquide, 99.997%) and CO_2 (Air Liquide, 99.998%) by connecting the gas outlet directly to the reaction chamber. On the other hand, methanol (Carlo Erba 99.8%) and pyridine (Carlo Erba, 99.7%) were introduced by bubbling with a nitrogen flow situated in a special glass apparatus.

XP spectra were recorded using a Perkin-Elmer Φ 5600ci spectrometer with a standard Al-Kα source (187.85 eV pass energy, 0.4 eV step, 0.05 s step^{-1} for surveys; 11.75 eV pass energy, 0.1 eV step, 0.1 s step^{-1} for detailed spectra.).

XRD patterns were obtained using a Bruker "D8 Advance" diffractometer with Bragg-Brentano geometry using a Cu Kα radiation (40 kV, 40 mA, $\lambda = 0.15406$ nm).

Thermogravimetric analysis (TGA) was carried out in a controlled atmosphere using the simultaneous differential techniques (SDT) 2960 of TA Instruments. The thermograms were recorded at 5 °C min^{-1} heating rates in air and in nitrogen flow. The temperature range was from RT to 800 °C.

BET surface area values were determined using a Gemini 2375 by Micromeritics Instrument Corporation.

3. Results and discussion

3.1. Characterization: nanoscale MgO by "aqueous wet chemical method" and "surfactant method"

In the samples prepared by the two methods, the peak positions of Mg 1s and Mg 2p (Table 1) and their shape (Fig. 1a and b, respectively) coincide and are consistent with the presence of Mg (II) in oxides [62–66]. The fitting procedure allows to observe in the Mg 1s signal, the presence of two contributions due to magnesium carbonate species (1304.6–1304.7 eV) and to magnesium oxide/hydroxide (1303.2–1303.3 eV) whereas in the Mg 2p peak (49.3–49.5 eV), only the contribution due to magnesium oxide/hydroxide is evident [62,63,66] thus suggesting the surface character of the carbonate species. Magnesium carbonate species are more evident in the samples obtained by means of the "surfactant method" (MgO-BR and MgO-TR, see Table 3).

In the O 1s spectra (Fig. 1c), two contributions at about 530.0 and 531.4–531.8 eV (Table 1) are evident; the fitting procedure reveals the presence of three contributions, one (529.6–529.8 eV) is attributed to the MgO and the others to magnesium hydroxide (531.1–531.3 eV) and carbonate species (532.2–532.3 eV) [62,63,65].

Table 1
XPS data (binding energy in eV) obtained for the MgO nanoscale samples prepared by different methods, compared with the reference values

Sample	Mg 1s oxide/hydroxide	Mg 1s carbonates	Mg 2p	O 1s oxide	O 1s hydroxide	O 1s carbonates
MgO-OX	1303.2	1304.7	49.3	529.7	531.3	532.3
MgO-TR	1303.3	1304.6	49.4	529.8	531.2	532.2
MgO-BR	1303.3	1304.6	49.5	529.7	531.1	532.2

MgO-OX: prepared by "aqueous wet chemical method"; MgO-TR: prepared by Triton X-100 "surfactant method"; MgO-BR: prepared by Brij 56 "surfactant method".
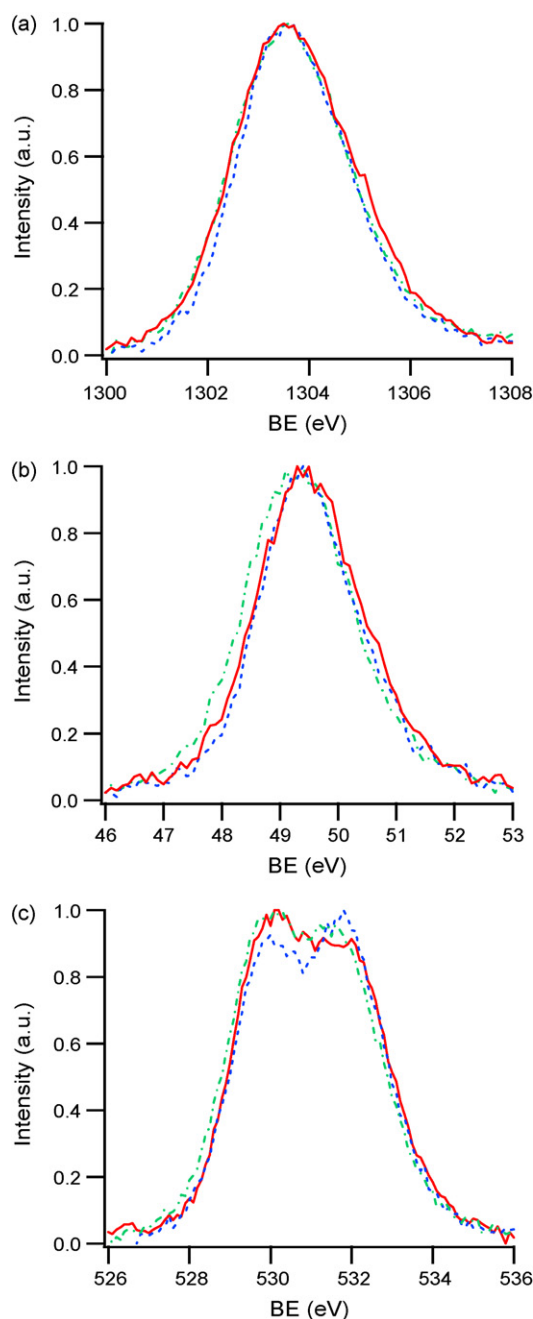

Fig. 1. XP spectra obtained at RT for the MgO powder samples; MgO-OX (——), MgO-BR (••••), MgO-TR (–·–·–). (a) Mg 1s (b) Mg 2p (c) O 1s.

The atomic compositions derived from the XP spectra are summarized in Table 2. The O/Mg atomic ratios are always higher than the stoichiometric values confirming the surface contamination; moreover, the O/Mg atomic ratio is always lower when obtained from Mg 2p peak, hence the presence of hydroxyls and carbonate species is prevalent on the surface [67]. It has also to be observed (Fig. 1, Tables 2 and 3) that the oxygen due to contaminants is more evident in the sample MgO-BR.

The XRD analysis shows only the presence of cubic MgO; using Scherrer's formula, [62,68] the mean crystallite dimensions were evaluated to lie between 13 nm (MgO-OX sample) and 16–18 nm (MgO-BR, MgO-TR samples).

The DRIFT spectra (Figs. 2 and 3), obtained as a function of temperature, show some differences between the MgO samples. First, in the MgO-OX sample spectra (Fig. 2a), between RT and 300 °C there is a strong, sharp absorption peak at ca. 3700 cm^{-1} characteristic of single νOH of Mg(OH)$_2$, [69–71]; this peak disappears at 350 °C and is almost insignificant in the samples obtained by means of the "surfactant method" (Fig. 3a). A relatively small peak at 3736 cm^{-1} is observed in all samples at high temperature (400 °C) and could be attributed to isolated OH-groups [70–72]. A broad band ranging from 3600 to 3000 cm^{-1} is evident in all the samples and particularly on MgO-OX. This band is most likely due to water molecules adsorbed on the sample surface [70] and to hydrogen-bound hydroxyl groups. This band is more evident at low temperatures and diminishes with increasing temperature. At RT the adsorbed moisture is less in the MgO-BR sample (Fig. 3a), but disappears more slowly than in the MgO-OX sample, thus indicating a stronger interaction. This result is consistent with XPS data that indicate a higher contamination under UHV conditions.

In Figs. 2b, 3b, a broad intense band between 1640–1300 cm^{-1} characteristic of mono- and bi-coordinated carbonate species (generated from the interaction with atmospheric CO$_2$) is observed [73]. In the MgO-BR sample, carbonate species tend to disappear at a lower temperature (350 °C), compared to the disappearing of these species at 400 °C in the MgO-OX sample. The aspects found in the samples and the behaviour observed at increasing temperatures suggest a different distribution of active sites.

The XPS and IR results indicate that the sites active toward the interaction with moisture are less numerous but stronger on the MgO-BR sample: in fact the corresponding IR signals are less intense in this sample but their decrease as a function of temperature is slower; moreover this is confirmed by XPS results indicating that the MgO-BR contaminants are more resistant at the UHV conditions. The site active toward the interaction

Table 2
XPS data (atomic compositions) obtained for the MgO nanoscale samples prepared by different methods

Sample	Mg 1s (%)			Mg 2p (%)			O/Mg	
	Mg	O	C	Mg	O	C	O/Mg 1s	O/Mg 2p
MgO-OX	30.2	56.6	13.2	33.5	53.9	12.6	1.8	1.6
MgO-TR	26.6	57.5	15.9	33.7	51.0	15.3	2.1	1.6
MgO-BR	17.9	55.4	26.7	26.3	49.7	24.0	3.0	1.9

MgO-OX: prepared by "aqueous wet chemical method"; MgO-TR: prepared by Triton X-100 "surfactant method"; MgO-BR: prepared by Brij 56 "surfactant method".

with carbon dioxide, in contrast, seems weaker: the carbonate species are removed at slightly lower temperature. The IR results concerning MgO-TR sample (not reported for sake of brevity) are almost identical to those obtained for MgO-BR.

The thermogram of the MgO-OX sample (Fig. 4) shows three thermal steps. The first step between 37 °C and 180 °C (6.5% loss) is attributed to the elimination of adsorbed moisture. The second step (12.3% loss), between 205 °C and 410 °C, is due to the conversion of some residual $Mg(OH)_2$ as well as to the elimination of carbonate species [73]. These results are consistent with the DRIFT analysis shown before. The third relatively small step (1.1% loss) at 500–600 °C is probably due to the elimination of some residual carbonate species. The smaller percent weight loss in the MgO-BR sample (first step: 2.6% and second step: 6.8%) (Fig. 4) confirms the suggestion of a different distribution of hydroxyl groups and active sites and particularly of a less relevant presence. The MgO-TR sample showed a relatively slight difference in the thermal analysis pattern compared to the MgO-BR sample such that the percent weight loss is higher in the two steps (first step 5.3% versus 2.6%; second step 9.0% versus 6.8%).

Finally, the specific surface area is influenced by the preparation procedure: the MgO-BR surface area ($22.62 \, m^2/g$) is lower than MgO-OX and MgO-TR surface areas (65.10 and $67.85 \, m^2/g$).

3.2. Reactivity: interaction with methanol

The DRIFT analysis was carried out both in methanol flow and after successive evacuation with nitrogen. Fig. 5 displays the IR spectra obtained after exposing the samples to methanol (for 3 min). In Figs. 6 to 8, the spectra collected after the nitrogen flow (for 5–10 min) are shown; this last procedure allows to avoid the contributions due to gas phase methanol and to better observe the signals due to the species that are rather strongly bonded to the surfaces.

As a general consideration, the IR spectra obtained at RT in methanol flow show a rather complex shape corresponding to the presence of several species. The spectral region corresponding to O—H stretching (Fig. 5a) suggests a severe perturbation of hydroxyl groups; in particular, new mono-coordinated hydroxyls are evident after exposure (signal at 3765–3770 cm^{-1}) thus indicating a dissociative chemisorption of methanol. This phenomenon is particularly evident for the MgO-OX sample suggesting the presence of more acidic/basic sites in MgO-OX. Signals attributed to the stretching of OH groups were already revealed after exposure to methanol; Tench et al., as an example, observed two contributions at 3740 and 3557 cm^{-1} [74]. Besides dissociated methanol, molecularly adsorbed and gas phase methanol are revealed by the broad bands in the C—O and C—H stretching regions (Fig. 5b and c) [75,76]. Moreover, the comparison between the spectra obtained in this region for the three samples suggests a more significant presence of gas phase and molecularly chemisorbed methanol in MgO-BR; this result is in agreement with a lower dissociation of methanol, as resulting from the IR region of OH stretching (Fig. 5a).

Note that a theoretical study by Branda et al. [22] postulated the possibility of a H-bond type interaction between surface oxygen anions and the hydrogen belonging to methanol. Moreover, oxygen and magnesium ions characterized by different coordinative insaturation exhibit different reactivity with respect to methanol: these sites are the only responsible of the methanol proton abstraction [22,25,26].

At RT (Fig. 5a) and 100 °C, the partial dissociation of methanol is also revealed by the C—O stretching signals around 1050–1060 cm^{-1} [77]. The comparison with literature data [78] suggests that the methoxy species are predominately bi-coordinated. It is also evident the C—O stretching contribution in this band at 1033 cm^{-1} corresponding to liquid-like methanol. As a general consideration, several methoxy species were observed after exposing MgO; at increasing temperature these species, whose C—O stretching frequencies range is around
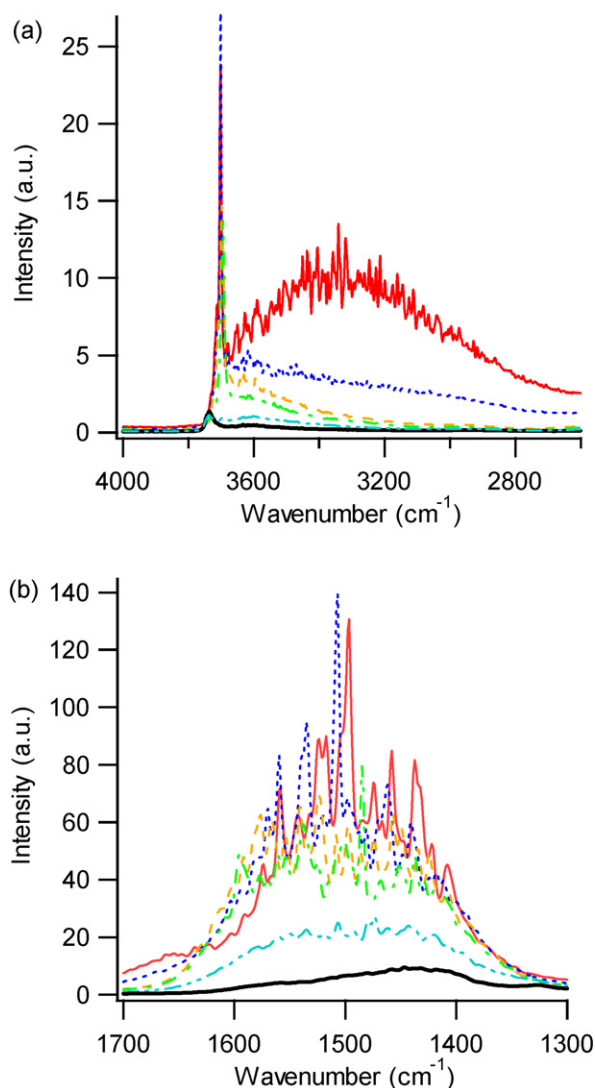
Table 3
XPS data (from fitting procedure) obtained for the MgO nanoscale samples prepared by different methods

Sample	Mg 1s (%)		O 1s (%)		
	Mg 1s oxide/hydroxide	Mg 1s carbonates	O 1s oxide	O 1s hydroxide	O 1s carbonates
MgO-OX	74	26	32	24	44
MgO-TR	65	35	30	24	46
MgO-BR	56	44	30	21	49

MgO-OX: prepared by "aqueous wet chemical method"; MgO-TR: prepared by Triton X-100 "surfactant method"; MgO-BR: prepared by Brij 56 "surfactant method".

Fig. 2. DRIFT profiles of the MgO-OX powder sample; RT (——), 100 °C (••••), 200 °C (▪ ▪ ▪), 300 °C (▬ ▪ ▬ ▪ ▬), 350 °C (-▪▪-▪▪-), and 400 °C (—). (a) Spectral range: 4000–2600 cm^{-1}, (b) spectral range: 1700–1300 cm^{-1}.

Fig. 3. DRIFT profiles of the MgO-BR powder sample; RT (——), 100 °C (••••), 200 °C (▪ ▪ ▪), 300 °C (▬ ▪ ▬ ▪ ▬), 350 °C (-▪▪-▪▪-), and 400 °C (—). (a) Spectral range: 4000–2600 cm^{-1}, (b) Spectral range: 1700–1300 cm^{-1}.

1060–1150 cm^{-1} (depending on the exposure conditions and on the MgO preparation procedure), show a different behaviour with respect to temperature [74,77,78]: in particular the signals characterized by higher stretching frequency can be observed until high temperature.

All the species except methoxy groups, are removed by N_2 evacuation (Fig. 6a); the position of the obtained signal (at about 1045 cm^{-1}) confirms its attribution to bi-coordinated methoxy groups.

At high temperatures, 300–400 °C, the dissociation leads to a new type of interaction where strongly bound mono-coordinated methoxy species (bands between 1120 and 1070 cm^{-1}) (Fig. 6b), prevail on the bi-coordinated ones. In particular a single signal at 1105 cm^{-1} is observed for MgO-OX whereas at least three contributions at 1115–1110, 1100–1090 and at about 1080 cm^{-1} are evident for MgO-BR and MgO-TR. This could suggest that at high temperatures "new" active sites (coordinatively unsaturated species) form probably as a consequence of the dehydroxyla-
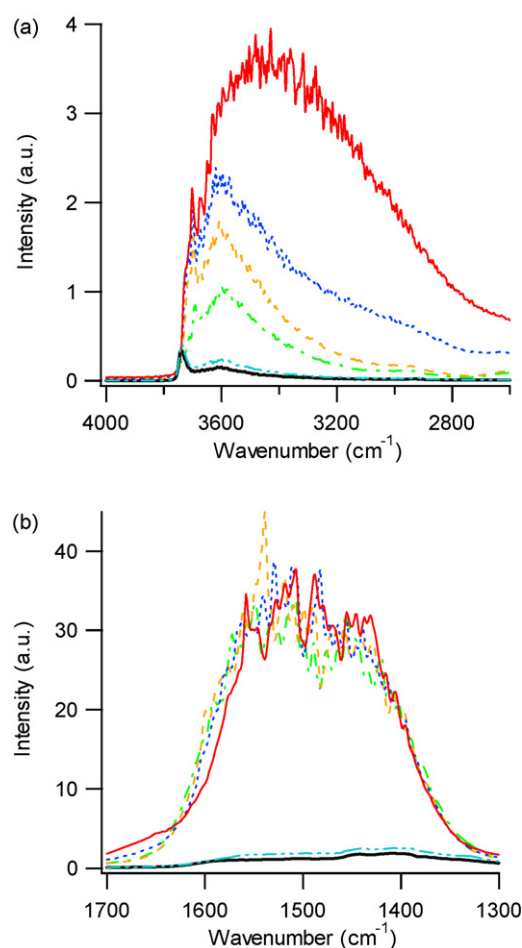
tion or the decomposition of carbonate species. The formation of these new sites is more evident in the surfactant samples in agreement with the DRIFT characterization results observed before where in practise, the MgO-BR and MgO-TR samples are observed to have less but relatively stronger active sites (as demonstrated by the presence of hydroxide groups at relatively high temperatures).
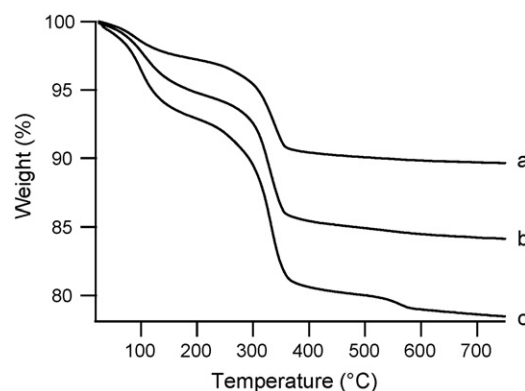

Fig. 4. TGA spectra of MgO samples obtained by different methods in air; (a) MgO-BR, (b) MgO-TR and (c) MgO-OX.
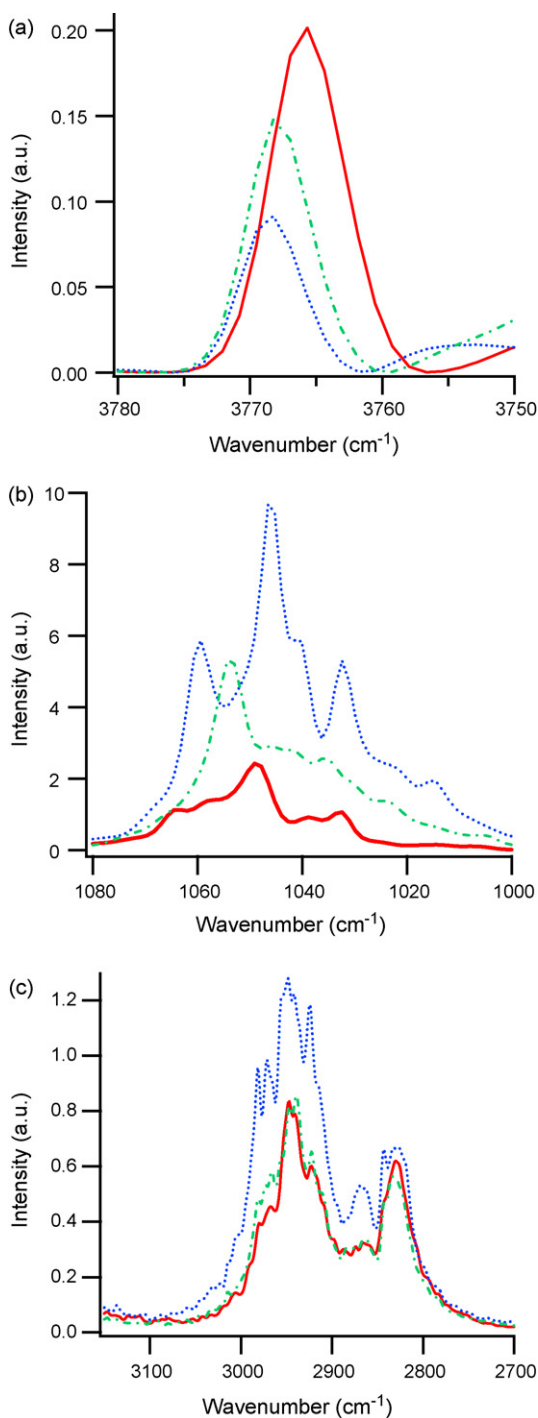
Fig. 5. DRIFT profiles of the MgO samples obtained after the exposure to methanol for 3 min (in nitrogen flow) at RT; MgO-OX (——), MgO-BR (••••), MgO-TR (—•—•—); (a) spectral range: 3780–3750 cm^{-1}, (b) spectral range: 1080–1000 cm^{-1}, (c) spectral range: 3200–2700 cm^{-1}.

Fig. 6. DRIFT profiles of the MgO samples obtained after the exposure to methanol (in nitrogen flow) and successively to N$_2$; MgO-OX (——), MgO-BR (••••), MgO-TR (—•—•—); (a) RT, spectral range: 1100–1000 cm^{-1}, (b) 300 °C, spectral range: 1150–1050 cm^{-1}.

As far as the oxidation products are concerned, methanol oxidation was observed to occur on MgO-BR/TR at rather low temperature (165 °C) giving rise to formaldehyde [79] or to formates [77] depending on the sample history, the exposure conditions, etc. Our IR data indicate that the samples form formic acid at RT [80]. This result is suggested by an intense signal centred at about 1670 cm^{-1} (Fig. 7a) as well as to the
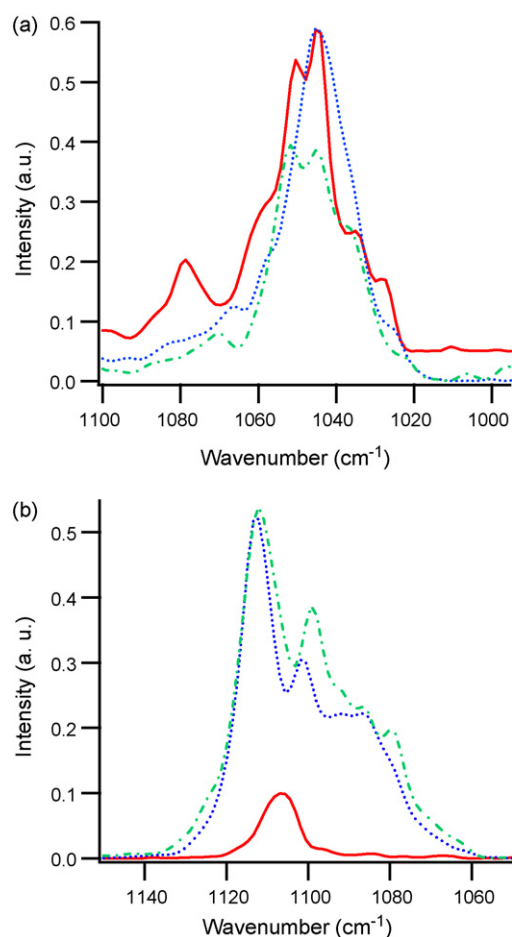
C–H stretching signal at around 2800 cm^{-1} (Fig. 7b). At higher temperature the exposure to methanol gives rise to different products depending on the preparation procedure. The peaks at about 1603 and 1625 cm^{-1} observed after exposing the samples to methanol at 300–400 °C and successively to N$_2$ (Fig. 8a), agree with the formation of bi-coordinated formates when considering the surfactant samples [77,81,82]. This is confirmed by the signals due to formates observed in the C–H stretching region (Fig. 8b). IR data indicate that the formation of formates is favoured at high temperatures. These formates are probably formed through the oxidation of methanol with reticular oxygen present on the surface and are rather stable because they persist after N$_2$ evacuation.

It is important to observe the absence of the C–H stretch in the MgO-OX sample suggesting the attribution of the peak at about 1600 cm^{-1} to bi-coordinated carbonates. This points out that at higher temperatures the MgO-OX sample possesses a different typology of sites with respect to the surfactant MgO samples and confirms that the preparation method greatly affects the properties of the active sites.

The CO and CO$_2$ are also noticed to form. The corresponding signals, in fact, are observed at high temperatures. In the
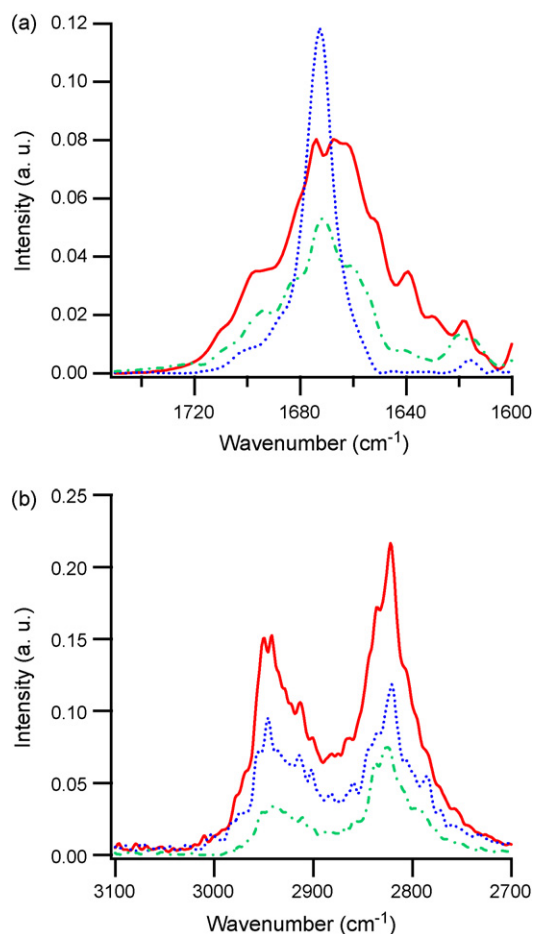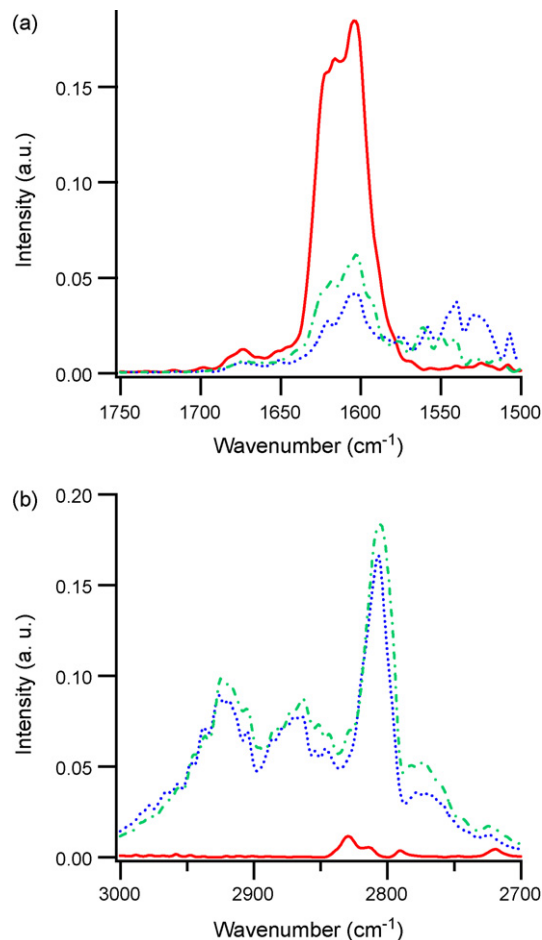
Fig. 7. DRIFT profiles of the MgO samples obtained after the exposure to methanol for 3 min (in nitrogen flow) and successively to N_2 at RT; MgO-OX (——), MgO-BR (••••), MgO-TR (—·—·—). (a) Spectral range: 1750–1600 cm^{-1}, (b) spectral range: 3100–2700 cm^{-1}.

MgO-OX sample, the CO starts to appear from 200 °C while CO_2 appears from 300 °C. On the other hand, in the "surfactant method" samples (MgO-BR and MgO-TR), both CO and CO_2 contributions start to be evident from 400 °C (Fig. 9). From Fig. 9 also, it could be noticed the more intense signals relative to the presence of CO_2 in the MgO-OX sample; moreover, at 400 °C MgO-OX induces only the formation of carbon dioxide.

The decrease in the formate and methoxy signals suggests that the possible mechanism for the formation of CO_2 is the oxidation of formate or CO with oxygen active sites. CO could be formed from methanol decomposition on the surface. Another interpretation comes from the reduction of CO_2 in which oxygen vacancies present on the surface of oxides takes away an oxygen from CO_2 to form CO indicating the relative high reactivity of the surface. This behaviour was already observed in several oxides [83–85].

Taking into consideration the surfactant samples, the CO_2 or CO produced does not generate any carbonates through the interaction with basic sites. This is particularly important for catalysis applications such that undesired products do not occupy the sites. After N_2 evacuation, these formed species are eliminated.

Fig. 8. DRIFT profiles of the MgO samples obtained after the exposure to methanol for 3 min (in nitrogen flow) and successively to N_2 at 400 °C; MgO-OX (——), MgO-BR (••••), MgO-TR (—·—·—). (a) Spectral range: 1700–1500 cm^{-1}, (b) spectral range: 3000–2700 cm^{-1}.

Concerning the surfactant samples and from the observations of methanol interaction with the surface, it could be said that at high temperatures, 300–400 °C, new active sites appear which favor the methanol dissociation and in a less extent oxidation.
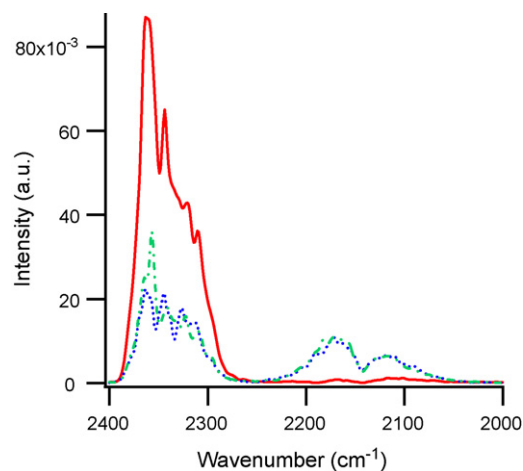

Fig. 9. DRIFT profiles of the MgO samples obtained after the exposure to methanol for 3 min at 400 °C; MgO-OX (——), MgO-BR (••••), MgO-TR (—·—·—). Spectral range: 2400–2000 cm^{-1}.

The different distribution of active sites could be responsible for the different reactivity with respect to methanol at high temperatures.

3.3. Reactivity: interaction with carbon monoxide (CO)

The interaction between CO and MgO is a very complex and investigated topic. This complexity originates from the formation of several different types of adsorbed species and from the great influence of the preparation procedure on the MgO surface and thus on the active sites.

The exposure of the samples to CO gives rise to several observations. At RT and 100 °C a small peak at 2057 cm^{-1} is observed in all cases (Fig. 10a); this signal is slightly more evident in the MgO-TR sample thus suggesting a higher presence of the active site responsible for this CO interaction. Earlier studies attributed the red-shifted signal to the formation of ketenic species through the interaction of a CO molecule with a $(O–C–O)^{2-}$ site originated by the adsorption of CO on a low-coordinated oxygen ion, O^{2-}_{LC} [33,50,52,53,86]. On the other hand, a complex interaction with the surface metal cations and the oxygen anions near neighbours was already hypothe-

sized to explain a similar behaviour for several oxides [87–89]. At elevated temperatures (300–400 °C) and in the MgO-OX sample only, it is noticed a blue shifted signal (2189 cm^{-1}) (Fig. 10b). At 400 °C, it is noticed a broadening of this peak suggesting different kinds of interactions with the surface. This last interaction is expected through coordination with Lewis acidic sites via a σ-donor bond [33,52,53] and suggests the formation of strong Lewis acidic site on the MgO-OX sample surface as a consequence of the heat treatment. In particular literature data suggest that the signal position agrees with the interaction with four-coordinated Mg^{2+} cations, Mg_{4C}^{2+} [33,50,52].

The obtained data suggest a significant influence of the sample history on the amount and distribution of the active sites, Mg_{LC}^{2+} and $Mg_{LC}^{2+}–O_{LC}^{2-}$ pairs, responsible of the interaction with CO [19]; moreover, the different distribution of active sites could be responsible for the different reactivity observed with respect to methanol.

The CO oxidation is revealed by the signals between 2300 and 2400 cm^{-1} due to carbon dioxide formation (Fig. 11). CO oxidation is not inconsistent with the proposed mechanism for CO interaction [33,50] in which O_{LC}^{2-} play an important role.

In the MgO-OX sample, the CO_2 starts to show up from 200 °C. The intensity is noticed to increase as temperature rises (200–400 °C), whereas for the MgO-TR and BR samples the CO_2 merely starts to appear at 300 °C. This suggests that MgO-OX has a higher reactivity towards oxidation. In all the samples, the obtained carbon dioxide is removed by a nitrogen flow and no formation of carbonate species was observed. This is a particularly important feature in catalysis where in most catalysts there is a tendency to be poisoned by the presence of CO. The MgO in this case interacts with CO forming "less" poisoning species, and supports the idea that MgO could be considered as a promising catalyst for decreasing the concentration of CO in exhaust gases. Another feature concerning CO oxidation is the formation of formates and formic acid [80]. These species, characterised by the bands at 1672 and 1625 cm^{-1} and by the peaks of CH stretching at 2830 cm^{-1}, are observed evidently at 400 °C (Fig. 11) and their formation is hypothesized to occur
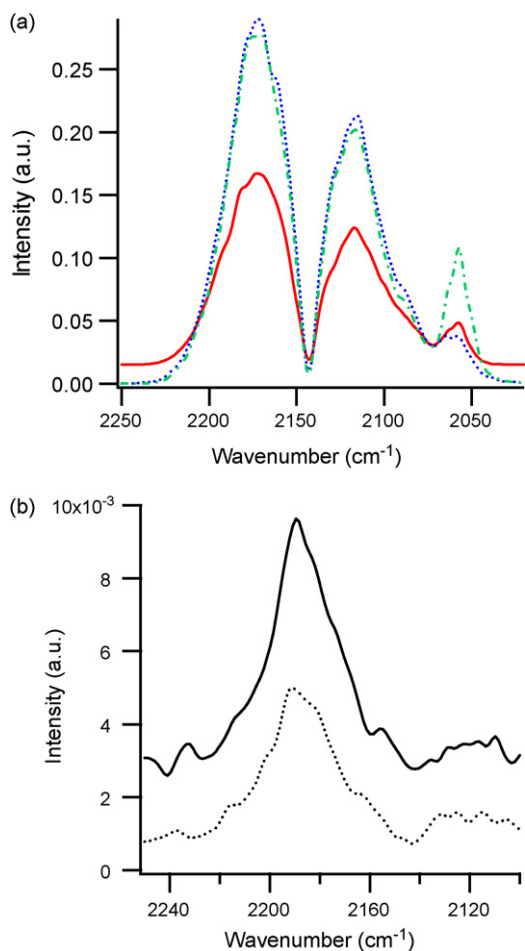

Fig. 10. DRIFT profiles of the MgO samples obtained after the exposure to CO; MgO-OX MgO-OX (——), MgO-BR (••••), MgO-TR (—·—·—). (a) RT spectral range: 2250–2020 cm^{-1}; (b) MgO-OX 300 °C (continuous line), 400 °C (dotted line); spectral range: 2250–2050 cm^{-1}.
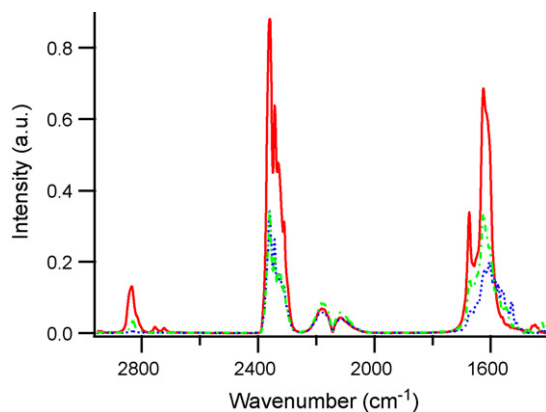

Fig. 11. DRIFT profiles of the MgO samples obtained after the exposure to CO at 400 °C; MgO-OX (——), MgO-BR (••••), MgO-TR (—·—·—). (a) Spectral range: 2500–1400 cm^{-1}, (b) spectral range: 3000–1400 cm^{-1}.

via the interaction of CO with surface hydroxyl groups. Also in this case, the MgO-OX sample exhibits the most intense peaks confirming the higher reactivity of MgO-OX.

3.4. Reactivity: interaction with carbon dioxide (CO_2) and pyridine (py)

In order to better understand the different aspects of MgO samples reactivity, it was intended to investigate the basic and acidic sites present through the interaction with CO_2 and py, respectively. Acid–base behaviour was already observed to be influenced by the sample history: mono- and bi-coordinated carbonate species and hydrogen carbonates were observed to form after exposing to carbon dioxide samples prepared and treated with different procedures [56–59,61,71]; moreover, it was observed that the reaction of carbon dioxide with MgO is rather limited, CO_2 only interacting with defect sites [57,90]. The active role of coordinatively unsaturated magnesium cations was already confirmed [6,7,12].

The DRIFT spectra obtained after exposing the MgO-OX and MgO-TR samples to CO_2 are shown in Fig. 12. The reactivity of MgO-BR does not differ significantly with respect to that of MgO-TR and thus the corresponding data are not reported.

In the MgO-OX sample at RT, two rather weak contributions at about $1620\,cm^{-1}$ and $1680\,cm^{-1}$ and a relatively small peak at $1387\,cm^{-1}$ (Fig. 12a) agree with the presence of bicarbonates species [56,59,71]. The absence of C-H stretching of formate species allows excluding their contribution to the peaks in the range $1700–1600\,cm^{-1}$. Bicarbonates could be the result of CO_2 interaction with residual free OH groups present on the surface. No peaks for mono-coordinated carbonate were detected. This result indicates the absence of coordinatively isolated oxygen anions and is in accordance with the high hydroxylation observed for this sample. With increasing temperature the signals due to carbonates get more intense; moreover, two signals at $1615\,cm^{-1}$ and $1297\,cm^{-1}$ suggest the formation of bi-coordinated carbonate species and thus of complex

sites constituted by a coordinatively unsaturated cation and a coordinatively unsaturated oxygen anion near neighbour.

At RT the MgO-TR sample shows a behaviour similar to MgO-OX but the peaks are more intense and mainly centred around $1650–1700\,cm^{-1}$, consistently with a higher presence of active hydroxyl groups.

At increasing temperature, a tail at about $1580–1600\,cm^{-1}$ is consistent with the formation of bi-coordinated carbonate species. The formation of bi-coordinated carbonates (and thus of complex acidic-basic sites) became prevalent at high temperatures (300–400 °C); bicarbonate species, however, never disappear (Fig. 12b). It is noteworthy observing that MgO-OX sample shows a more evident presence of bicarbonate and bi-coordinated species at 300–400 °C. Moreover, at high temperatures some mono-coordinated carbonates appear, as evidenced by the shoulder at about $1520\,cm^{-1}$ [59]. The interaction of carbon dioxide with coordinatively unsaturated oxygen anions (obtained as a consequence of the surface dehydroxylation) is a possible interpretation for the formation of the mono-

Fig. 13. DRIFT profiles obtained after a prolonged (15 min) exposure to pyridine at RT; (a) MgO-OX sample (▬) Spectral range: $1800–1400\,cm^{-1}$. (b) MgO-OX sample (▬) Spectral range: $3750–3650\,cm^{-1}$. (c) MgO-TR sample (••••) Spectral range: $1800–1400\,cm^{-1}$.
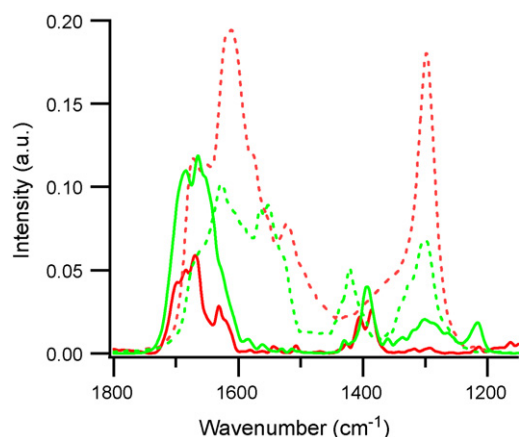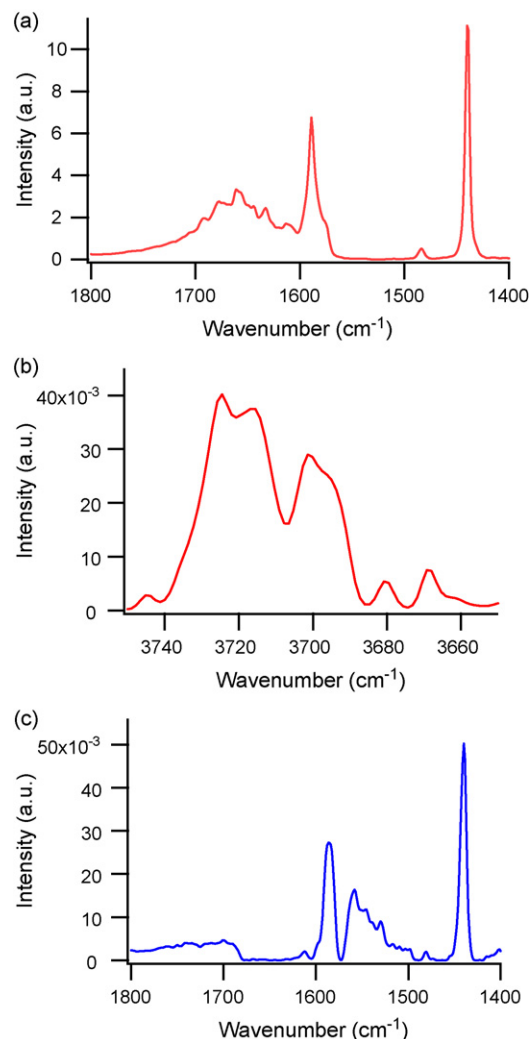

Fig. 12. DRIFT profiles of the MgO samples obtained after the exposure to CO_2: MgO-OX RT (red continuous line), MgO-OX 400 °C (red dotted line); MgO-TR RT (green continuous line), MgO-TR 400 °C (green dotted line). Spectral range: $1800–1150\,cm^{-1}$. (For interpretation of the references to colour in this figure legend, the reader is referred to the web version of the article.)

coordinated carbonate species. In comparison between the two samples, the carbonates formed on the MgO-TR tend to remain after N_2 evacuation. This indicates a relatively stronger CO_2 interaction. The presence of basic sites on MgO is commonly attributed to surface O^{2-} anions: differently coordinated O^{2-} sites must be responsible for basic sites of different strengths [59]. No significant differences have been observed between the two samples prepared by using different surfactants.

Finally, it is important to note that the CO_2 conversion to CO was never observed thus suggesting that the formation of CO after exposure to methanol cannot be attributed to this phenomenon.

Regarding the Py adsorption experiment, several studies claimed that MgO samples obtained by different preparation procedures are characterized by different acidity [40,59,61]. The DRIFT experiments were performed at RT under N_2 atmosphere.

In the MgO-OX sample after a prolonged exposure to py (Fig. 13a), two major peaks at $1585\,cm^{-1}$ and $1439\,cm^{-1}$ attributed to liquid-like py are noticed [60–61,91]. It is also noticed the presence of a broad band at $1661\,cm^{-1}$ attributed to the interaction with strong acidic sites [92] however the formation of oxidation products could not be excluded [93]. The sharp peak at $3724\,cm^{-1}$ (Fig. 13b), is attributed to the υOH as a result of a possible rearrangement of the hydroxyl groups after the adsorption of py [60]. On the other hand, in the TR sample (Fig. 13c), much less intense peaks are noticed at $1586\,cm^{-1}$ and $1439\,cm^{-1}$ suggesting that pyridine is merely in liquid-like form; a weak and broad signal around $1550\,cm^{-1}$ is in agreement with the formation of traces of pyridinium ion and thus with the presence of Brønsted acidic sites (similar results have been obtained on the MgO-TR sample). From these results, it could be deduced that the acidic/basic sites distribution is influenced by the preparation procedure. It is noteworthy saying that in all the investigated samples the interaction with py is a slow process as the peaks are seen only after a prolonged exposure.

4. Conclusions

To study the influence of the synthesis procedure, nanoscale magnesium oxide was prepared by two different procedures: "aqueous wet chemical method" and "surfactant method"; moreover, the effect of the surfactant was investigated taking into consideration two different surfactant (Brij 56 and Triton 100-X).

XRD patterns indicate the presence of cubic MgO. The mean crystallite sizes evaluated by means of Scherrer's equation are around 13–18 nm.

XPS analysis showed that the samples are homogeneous and with a certain hydroxylation on the surface. On the other hand, the samples showed differences in the interaction with the atmosphere (CO_2 and moisture) as evidenced by the DRIFT analysis. These differences suggest the presence of different sites and hence a different reactivity.

The influence of the preparation procedure on the reactivity was confirmed through the interaction with probe molecules (methanol and carbon monoxide).

At low temperatures (RT-200 °C), methanol interacts molecularly and dissociatively with all the samples; dissociative interaction increases with increasing temperature. IR data suggest that the sample obtained by "aqueous wet chemical method" is relatively more active in the dissociation of methanol especially at RT. At higher temperatures (300–400 °C), different oxidation products (formates and formic acid, CO and CO_2) were observed. Moreover the sample prepared by "aqueous wet chemical method" is the most active in oxidation.

All the samples interact with CO at RT causing a red-shift of the signal characteristic of carbon monoxide; this interaction is more evident in the MgO-TR sample. A blue-shifting interaction is observed, at high temperature, on the sample obtained by "aqueous wet chemical method". CO oxidation produces CO_2, formic acid and formates starting from 200 °C in the "aqueous wet chemical method sample" and at relatively higher temperatures in the "surfactant method" samples.

The interaction with CO_2 and pyridine revealed a different distribution of acidic/basic active sites for the samples synthesized with "aqueous wet chemical method" and "surfactant method". No significant difference, in contrast, has been marked between the samples prepared from different surfactants.

Appendix A. Supplementary data

Supplementary data associated with this article can be found, in the online version, at doi:10.1016/j.molcata.2007.04.039.

References

[1] R.E. Kirk, D.F. Othmer, M. Grayson, D. Eckroth Kirk-Othmer, Encyclopaedia of Chemical Technology, vol. 14, John Wiley and Sons, 1981.
[2] B.Q. Xu, J.M. Wie, H.Y. Wang, K.Q. Sun, Q.M. Zhu, Catal. Today 68 (2001) 217.
[3] K. Klabunde, Nanoscale Materials in Chemistry, Wiley Interscience, 2001.
[4] A. Khaleel, P.N. Kapoor, K.J. Klabunde, Nanostruct. Mater. 11 (1999) 459.
[5] M. Fernandez-Garcia, A. Martinez-Arias, J.C. Hanson, J.A. Rodriguez, Chem. Rev. 104 (2004) 4063.
[6] T. Ito, H. Kobayashi, T. Tashiro, Il Nuovo Cimento 19 (1997) 1695.
[7] A. Markovits, J. Ahdjoudj, C. Minot, Il Nuovo Cimento 19 (1997) 1719.
[8] H. Yamamoto, N. Watanabe, A. Wada, K. Domen, J. Chem. Phys. 106 (1997) 4734.
[9] L. Chen, R. Wu, N. Kioussis, Q. Zhang, Chem. Phys. Lett. 290 (1998) 255.
[10] D. Ochs, M. Brause, W. Maus-Friedrichs, V. Kempter, J. Electr. Spectr. Rel. Phenom. 88–91 (1998) 757.
[11] A.G. Pelmenschikov, G. Morosi, A. Gamba, S. Coluccia, J. Phys. Chem. B 102 (1998) 2226.
[12] J. Ahdjoudj, A. Markovits, C. Minot, Catal. Today 50 (1999) 541.
[13] X. Lu, X. Xu, N. Wang, Q. Zhang, J. Phys. Chem. B 104 (2000) 10024.
[14] A. Pelmenschikov, G. Morosi, A. Gamba, S. Coluccia, G. Martra, L.G.M. Pettersson, J. Phys. Chem. B 104 (2000) 11497.
[15] J.A. Rodriguez, T. Jirsak, S. Sambasivan, D. Fischer, A. Maiti, J. Chem. Phys. 112 (2000) 9929.

[16] J.A. Snyder, D.R. Alfonso, J.E. Jaffe, Z. Lin, A.C. Hess, M. Gutowski, J. Phys. Chem. B 104 (2000) 4717.

[17] R. Soave, G. Pacchioni, Chem. Phys. Lett. 320 (2000) 345.

[18] A. Damin, R. Dovesi, A. Zecchina, P. Ugliengo, Surf. Sci. 479 (2001) 255.

[19] G. Martra, T. Cacciatori, L. Marchese, J.S.J. Hargreaves, I.M. Mellor, R.W. Joyner, S. Coluccia, Catal. Today 70 (2001) 121.

[20] J.A. Rodriguez, T. Jirsak, M. Pérez, A. Maiti, J. Chem. Phys. 114 (2001) 4186.

[21] A. Zecchina, D. Scarano, S. Bordiga, G. Spoto, C. Lamberti, Adv. Catal. 46 (2001) 265, and reference therein.

[22] M.M. Branda, J.E. Peralta, N.J. Castellani, R.H. Contreras, Surf. Sci. 504 (2002) 235.

[23] S. Krischok, O. Höfft, V. Kempter, Nucl. Inst. Methods Phys. Res. B 193 (2002) 466.

[24] P. Ugliengo, A. Damin, Chem. Phys. Lett. 366 (2002) 683.

[25] M.M. Branda, P.G. Belelli, R.M. Ferullo, C.J. Castellani, Catal. Today 85 (2003) 153.

[26] M.M. Branda, R.M. Ferullo, P.G. Belelli, C.J. Castellani, Surf. Sci. 527 (2003) 89.

[27] E.J. Karlsen, M.A. Nygren, L.G.M. Pettersson, J. Phys. Chem. B 107 (2003) 7795.

[28] P. Martino, M. Chiesa, M.C. Paganini, E. Giamello, Surf. Sci. 527 (2003) 80.

[29] G. Spoto, E. Gribov, A. Damin, G. Ricchiardi, A. Zecchina, Surf. Sci. 540 (2003) L605.

[30] Y. Xu, J. Li, Y. Zhang, W. Chen, Surf. Sci. 525 (2003) 13.

[31] J. Rudberg, M. Foster, J. Phys. Chem. B 108 (2004) 18311.

[32] W.F. Schneider, J. Phys. Chem. B 108 (2004) 273.

[33] G. Spoto, E.N. Gribov, G. Ricchiardi, A. Damin, D. Scarano, S. Bordiga, C. Lamberti, A. Zecchina, Progr. Surf. Sci. 76 (2004) 71, and references therein.

[34] H.C. Liang Septimus, D. Gay Ian, Langmuir 1 (1985) 593.

[35] K.J. Klabunde, J. Stark, O. Koper, C. Mohs, D.G. Park, S. Decker, Y. Jiang, I. Lagadic, D. Zhang, J. Phys. Chem. 100 (1996) 12142.

[36] J. Jiu, K. Kurumada, M. Tanigaki, M. Adachi, S. Yoshikawa, Mater. Lett. 58 (2003) 44.

[37] A.V. Chadwick, I.J.F. Poplett, D.T.S. Maitland, M.E. Smith, Chem. Mater. 10 (1998) 864.

[38] X. Bokhimi, A. Morales, M. Portilla, A. García-Ruiz, Nanostruct. Mater. 12 (1999) 589.

[39] X. Bokhimi, A. Morales, J. Solid State Chem. 115 (1995) 411.

[40] T. López, R. Gómez, J. Navarrete, E. López-Salinas, J. Sol-Gel Sci. Technol. 13 (1998) 1043.

[41] S. Utamapanya, K.J. Klabunde, J.R. Schlup, Chem. Mater. 3 (1991) 175.

[42] Y. Ding, G. Zhang, H. Wu, B. Hai, L. Wang, Y. Qian, Chem. Mater. 13 (2001) 435.

[43] R.M. Laine, C.R. Bickmore, D.R. Treadwell, K.F. Waldner, U.S. Pat. US 5,958,361, 1999.

[44] M. El-Shall, W. Slack, W. Vann, D. Kane, D. Hanley, J. Phys. Chem. 98 (1998) 3067.

[45] J.S. Matthews, O. Just, B. Obi-Johnson, W.S. Rees Jr., Chem. Vap. Deposition 6 (2000) 129.

[46] J.J. Helble, J. Aerosol Sci. 29 (1998) 721.

[47] A. Bhargava, J. Alarco, I. Mackinnon, D. Page, A. Ilyushechkin, Mater. Lett. 34 (1998) 133.

[48] P. Talbot, J.A. Alarco, G.A. Edwards, WO 02/42201 (Cl. C01B13/36), 2002.

[49] Methanol oxidation reactions on oxide surfaces are very sensitive to the nature of active catalytic site. The methanol oxidation product at low conversions reflects the nature of the surface active sites: redox sites yields formaldehyde through oxidative dehydrogenation, CO_2 when basic sites are also present and the existence of Lewis and Brønsted acid sites leads to the dehydration of the oxidised carbon species giving dimethyl ether. See, as an example, M. Badlani, I.E. Wachs, Catal. Lett., 75 (2001) 137.

[50] T. Ito, H. Kobayashi, Recent Res. Dev. Phys. Chem. 1 (1997) 289.

[51] M.I. Zaki, H. Knözinger, Spectrochim. Acta 43A (1987) 1455.

[52] M.A. Babaeva, D.S. Bystrov, A.Yu. Kovalgin, A.A. Tsyganenko, J. Catal. 123 (1990) 396.

[53] M.A. Babaeva, A.A. Tsyganenko, React. Kinet. Catal. Lett. 34 (1987) 9.

[54] L. Guczi, New Trends in CO Activation, Elsevier, Amsterdam, 1991.

[55] Y. Yanagisawa, K. Takaoka, S. Yamabe, T. Ito, J. Phys. Chem. 99 (1995) 3704.

[56] R. Philipp, K. Fujimoto, J. Phys. Chem. 96 (1992) 9035.

[57] X. Carrier, C.S. Doyle, T. Kendelewicz, G.E. Brown Jr., Surf. Rev. Lett. 6 (1999) 1237.

[58] A. Auroux, A. Gervasini, J. Phys. Chem. 94 (1990) 6371.

[59] M.A. Aramendía, V. Boráu, C. Jiménez, J.M. Marinas, A. Porras, F.J. Urbano, J. Mater. Chem. 6 (1996) 1943.

[60] C. Martin, I. Martin, V. Rives, J. Mol. Catal. 73 (1992) 51.

[61] G.A.H. Mekhemer, S.A. Halawy, M.A. Mohamed, M.I. Zaki, J. Phys. Chem. B 108 (2004) 13379.

[62] D.K. Aswal, K.P. Muthe, S. Tawde, S. Chodhury, N. Bagkar, A. Singh, S.K. Gupta, J.V. Yakhmi, J. Cryst. Growth 236 (2002) 661.

[63] S. Ardizzone, C.L. Bianchi, M. Fadoni, B. Vercelli, Appl. Surf. Sci. 119 (1997) 253.

[64] S.M. Lee, T. Ito, H. Murakami, J. Mater. Res. 17 (2002) 1914.

[65] NIST X-ray Photoelectron Spectroscopy Standard Reference Database 20, Version 3.4 (Web Version).

[66] S. Altieri, S.F. Contri, S. Agnoli, S. Valeri, Surf. Sci. 566/568 (2004) 1071.

[67] Because of the different kinetic energy, escape depth is higher for Mg 2p than Mg 1s photoelectrons, see as an example C.S. Fadley in Electron Spectroscopy Theory, Techniques and Applications; C.R. Brundle, A.D. Baker (Eds.), Academic Press, 1978, Chap. 1.

[68] H.P. Klug, L.E. Alexander, X-ray Diffraction Procedures, second ed., Wiley Interscience, New York, 1974.

[69] H.W. Van der Marel, H. Beutelspacher, Atlas of Infrared Spectroscopy of Clay Minerals and Their Admixtures, Elsevier Scientific Publishing Co., New York, 1976.

[70] M.A. Aramendía, V. Boráu, C. Jiménez, A. Marinas, J.M. Marinas, J.A. Navío, J.R. Ruiz, F. Urbano, J. Colloids Surf., A: Physicochem. Eng. Aspects 234 (2004) 17.

[71] J.V. Stark, D.G. Park, I. Lagadic, K.J. Klabunde, Chem. Mater. 8 (1996) 1904.

[72] O. Diwald, M. Sterrer, E. Knözinger, Phys. Chem. Chem. Phys. 4 (2002) 2811.

[73] E. Alvarado, L.M. Torres-Martinez, A.F. Fuentes, P. Quintana, Polyhedron 19 (2000) 2345.

[74] J.A. Tench, D. Giles, J.F. Kibblewhite, J. Trans. Faraday Soc. 67 (1971) 854.

[75] G. Herzberg, Infrared and Raman Spectra of Polyatomic Molecules, Van Nostrand, New York, 1949.

[76] M. Falk, E. Whalley, J. Chem. Phys. 34 (1961) 1554.

[77] J. Kondo, Y. Sakata, K.I. Maruya, K. Tamaru, T. Onishi, Appl. Surf. Sci. 28 (1987) 475.

[78] M. Bensitel, O. Saur, J.C. Lavalley, Mater. Chem. Phys. 28 (1991) 309.

[79] D.C. Foyt, J.M. White, J. Catal. 47 (1977) 260.

[80] R.C. Millikan, K.S. Pitzer, J. Am. Chem. Soc. 80 (1958) 3515.

[81] K. Teramura, T. Tanaka, H. Ishikawa, Y. Kohno, T. Funabiki, J. Phys. Chem. B 108 (2004) 346.

[82] G.W. Wang, H. Hattori, J. Chem. Soc. Faraday Trans. I 80 (1984) 1039.

[83] G.B. Raupp, J.A. Dumesic, J. Phys. Chem. 89 (1985) 5240.

[84] M. Casarin, D. Falcomer, A. Glisenti, A. Vittadini, Inorg. Chem. 42 (2003) 436.

[85] M.M. Natile, A. Glisenti, Chem. Mater. 14 (2002) 3090.

[86] T. Tashiro, J. Ito, R.-B. Sim, K. Miyazawa, E. Hamada, D. Toi, H. Kobayashi, T. Ito, J. Phys. Chem. 99 (1995) 6115.

[87] F. Grillo, M.M. Natile, A. Glisenti, Appl. Catal., B: Environ. 48 (2004) 267.

[88] M. Casarin, C. Maccato, A. Vittadini, J. Phys. Chem. B 106 (2002) 795.

[89] T. Chiong, A. Davydov, Russ. J. Phys. Chem. 63 (1989) 152.

[90] S.M. Ward, J. Braslaw, R.L. Gealer, Thermochim. Acta 64 (1983) 107.

[91] L. Corrsin, B.J. Fax, R.C. Lord, J. Chem. Phys. 21 (1953) 1170.

[92] G. Busca, Catal. Today 41 (1998) 191.

[93] M.I. Zaki, M.A. Hasan, F.A. Al-Sagheer, L. Pasupulety, Colloids Surf., A 190 (2001) 261.